Geochemistry, Geophysics, Geosystems

RESEARCH ARTICLE
10.1029/2019GC008311

Key Points:
- The submarine volcano Ahyi erupted for 2 weeks in April–May 2014 and was recorded by regional seismometers and distant hydrophones
- The eruption was characterized by several thousand explosions and occasional tremor at the beginning and end of the eruptive period
- Repeat bathymetry reveals a new summit crater and a new, large landslide chute on the south flank

Supporting Information:
- Supporting Information S1

Correspondence to:
G. Tepp,
gtepp@usgs.gov

Citation:
Tepp, G., Chadwick, W. W., Jr, Haney, M. M., Lyons, J. J., Dziak, R. P., Merle, S. G., et al (2019). Hydroacoustic, seismic, and bathymetric observations of the 2014 submarine eruption at Ahyi Seamount, Mariana Arc. *Geochemistry, Geophysics, Geosystems*, *20*, 3608–3627. https://doi.org/10.1029/2019GC008311

Received 6 MAR 2019
Accepted 26 JUN 2019
Accepted article online 2 JUL 2019
Published online 26 JUL 2019

Hydroacoustic, Seismic, and Bathymetric Observations of the 2014 Submarine Eruption at Ahyi Seamount, Mariana Arc

Gabrielle Tepp[1], William W. Chadwick Jr[2], Matthew M. Haney[1], John J. Lyons[1], Robert P. Dziak[2], Susan G. Merle[3], David A. Butterfield[4], and Charles W. Young III[5]

[1]U. S Geological Survey, Alaska Volcano Observatory, Anchorage, AK, USA, [2]NOAA Pacific Marine Environmental Laboratory, Newport, OR, USA, [3]CIMRS, Oregon State University, Newport, OR, USA, [4]JISAO, and NOAA PMEL, University of Washington, Seattle, WA, USA, [5]Coral Reef Ecosystem Program, NOAA Pacific Islands Fisheries Science Center, Honolulu, HI, USA

Abstract Ahyi seamount, a shallow submarine volcano in the Northern Mariana Islands, began erupting on 23 April 2014. Hydroacoustic eruption signals were observed on the regional Mariana seismic network and on distant hydrophones, and National Oceanic and Atmospheric Administration (NOAA) scuba divers working in the area soon after the eruption began heard and felt underwater explosion sounds. The NOAA crew observed yellow-orange bubble mats along the shore of neighboring Farallon de Pájaros Island, but no other surface manifestations of the eruption were reported by the crew or observed in satellite data. Here, we detail the eruption chronology and its morphologic impacts through analysis of seismic and hydroacoustic recordings and repeat bathymetric mapping. Throughout the 2-week-long eruption, Ahyi produced several thousand short, impulsive hydroacoustic signals that we interpret as underwater explosions as well as tremor near the beginning and end of the sequence. The initial tremor, which occurred for 2 hr, is interpreted as small phreatomagmatic explosions. This tremor was followed by a 90-min pause before the characteristic impulsive signals began. Occasional tremor (lasting up to a few minutes) during the last 1.5 days of the eruption is interpreted as more sustained eruptive activity. Bathymetric changes show that a new crater, about 150 m deep, formed near the former summit and a large landslide chute formed on the southeastern flank. Comparing to other geophysically detected submarine eruptions, we find that the signals from the 2014 Ahyi eruption were more similar to those from other shallow or at-surface submarine eruptions than those at deep (>500 m) eruptions.

Plain Language Summary Ahyi seamount, a shallow submarine volcano in the Commonwealth of the Northern Mariana Islands (CNMI), began erupting on 23 April 2014. The U.S. Geological Survey first noticed signs of the eruption during a routine data check on 24 April, while National Oceanic and Atmospheric Administration scuba divers working in the area heard and felt underwater explosion sounds. We analyze recordings of the eruption on the CNMI seismic network and on hydrophones located near Wake Island to detail how the eruption unfolded. The eruption started with about 2 hr of tremor from magma explosively interacting with water. After a 90-min pause, short (up to a few seconds) explosions began and continued for 2 weeks. During the last 1.5 days of the eruption, longer tremor signals (up to a few minutes) from more sustained degassing eruptions occurred along with the short explosions. A comparison of bathymetric maps made before and after the eruption shows that the explosions formed a new crater 150 m deep near the summit and that a landslide chute formed on the southeastern flank. The seismic and hydroacoustic signals from the Ahyi eruption are more similar to those from eruptions at other shallow or at-surface seamounts than to those from deep (>500 m) eruptions.

1. Introduction

Submarine volcanism is estimated to comprise ~75% of worldwide magmatic activity (Crisp, 1984). However, submarine eruptions are difficult to detect and characterize due to the lack of widespread geophysical sensors in the oceans and few land-based instruments on sparsely separated islands. About half of the geophysical detections of previous submarine eruptions were made with distant (>500 km) hydrophones or seismic stations. Efficient propagation of hydroacoustic waves (herein "T-phases") allows these distant

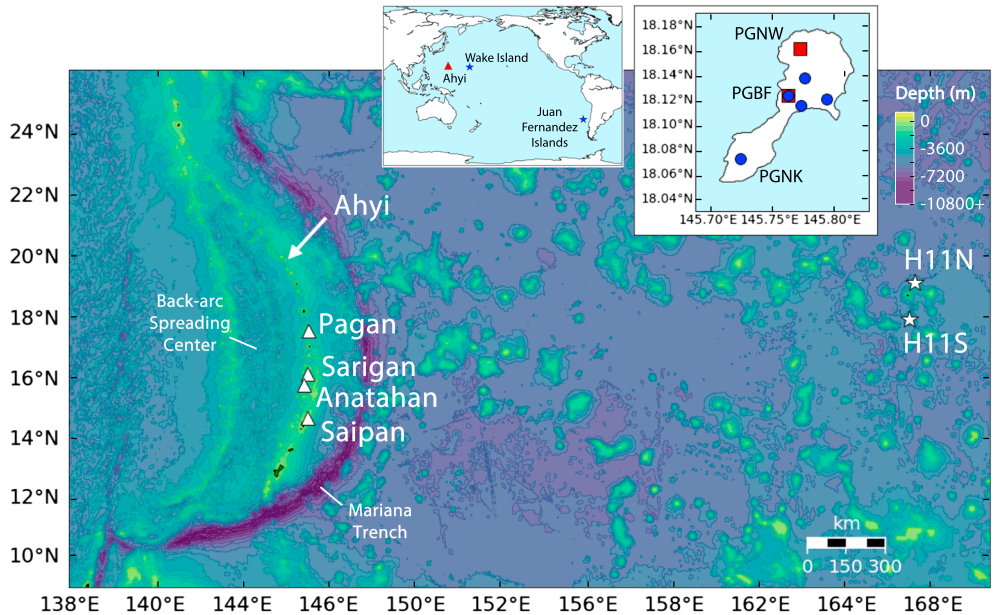

Figure 1. Regional map of the Commonwealth of the Northern Mariana Islands showing the location of Ahyi volcano. Islands with Northern Mariana Islands network seismic stations operating during the eruption are indicated by triangles. The Wake Island hydrophone arrays (H11N and H11S) are marked with white stars and labels. Left inset shows locations of Ahyi (red triangle) and the hydrophone arrays (blue stars, labeled). Right inset shows Pagan Island with blue dots marking seismometers operating during the eruption and red squares marking infrasound arrays. Seismic and infrasound stations on Pagan Island that are referred to in the text are labeled.

detections to be made. T-phases in the deep ocean can travel through the SOund-Fixing And Ranging (SOFAR) channel, leading to slower decline in energy due to cylindrical spreading of the channelized waves rather than the spherical spreading typical of seismic body waves. The water column is also less attenuating than the solid Earth. Island-based seismic stations are capable of detecting hydroacoustic T-phases that convert to seismic phases (herein "converted T-phases") as they reach land under the right circumstances (Talandier & Okal, 1998).

On 23 April 2014, Ahyi Seamount (hereafter, Ahyi), a shallow submarine volcano with a summit depth of ~75 m located in the Commonwealth of the Northern Mariana Islands (CNMI), began erupting for the first time since 2001. The eruption was marked by a 2-week-long series of thousands of short-duration impulsive acoustic events along with occasional periods of tremor, which were detected by the CNMI seismic network on nearby islands and on distant hydrophones near Wake Island and the Juan Fernandez Islands, Chile (Figure 1). Initially, the location of the seismoacoustic activity could only be localized as coming from somewhere north of Pagan Island due to geometric limitations of the real-time, island-based seismic network. However, scuba divers on a National Oceanic and Atmospheric Administration (NOAA) expedition monitoring coral reefs in the northern CNMI during late April reported hearing and feeling the underwater explosions and concussions while working at the neighboring island of Farallon de Pájaros (FdP, located only ~20 km NW of Ahyi) and later near Maug Islands (~50 km SE). Detections on the Wake Island hydrophone arrays further constrained the activity to the region near FdP Island. Soon after the eruption ended in early May, another NOAA expedition conducted bathymetric mapping and surveyed the water column around Ahyi for hydrothermal plumes (Buck et al., 2018). This survey found evidence that Ahyi was the likely source of the eruption. A later expedition in December 2014 collected a more complete bathymetric resurvey of the seamount. We describe the April–May 2014 eruption of Ahyi and its morphologic consequences using hydroacoustic, seismic, and bathymetric data. The direct observations of the eruption add further detail to our interpretations.

2. Background

The Mariana Arc is a chain of active volcanoes, mostly submarine, resulting from the Pacific Plate subducting under the Philippine Sea Plate (Stern, 2002). The volcanic chain is located west of the Mariana Trench

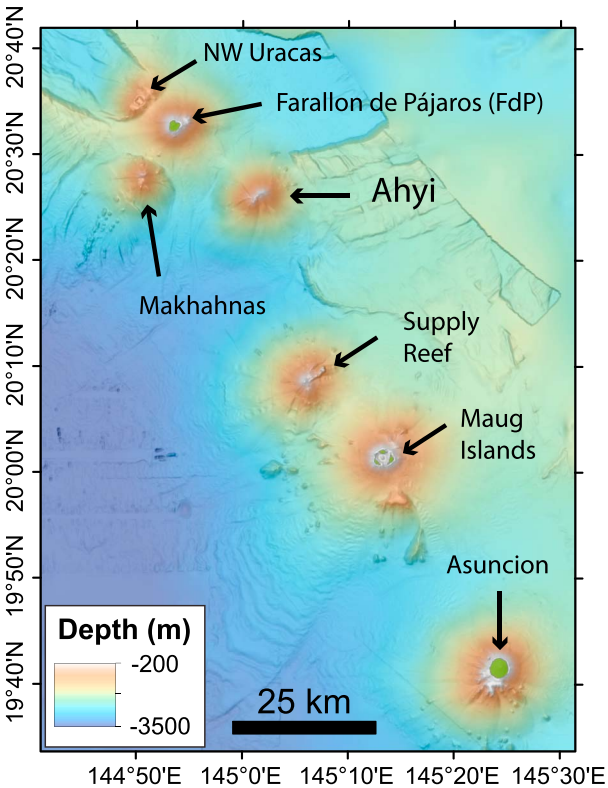

Figure 2. Bathymetric map of the area around Ahyi Seamount, showing the islands (shown in green) of Farallon de Pájaros (FdP), Maug, and Asuncion and the neighboring seamounts of Supply Reef, Makhahnas, and NW Uracas. All are active volcanoes.

and east of the back-arc spreading center (Figure 1). Six of the nine volcanic islands have been historically active, dating back to the 1800s. Around 60 seamounts have been identified in the arc, with about one-third of them hosting active hydrothermal systems (Baker et al., 2008; Embley et al., 2007; Resing et al., 2009). Six of the seamounts are known to have erupted historically (e.g., Embley et al., 2006; Embley et al., 2014). Some of the volcanic islands and many of the seamounts (including Ahyi) are located within the Mariana Trench Marine National Monument. Ahyi Seamount is located ~18 km southeast of the historically active, subaerial FdP (also known as Uracas) volcano, the northernmost island in the Mariana Arc (Figure 2). Other nearby seamounts include Makhahnas ~19 km to the west and Supply Reef ~33 km to the south, both of which have been historically active.

Several occurrences of submarine volcanic activity have been detected in the Ahyi-Supply Reef region since the 1960s. Most of the observations have come from distant hydrophone or seismic recordings with location errors too large to associate the activity with any particular seamount (e.g., McCreery et al., 1989; Sugioka et al., 2005). In some cases, direct observations of activity, such as discolored water on the ocean surface, helped to identify the source. The last confirmed eruption of Ahyi was in 2001, though it was short-lived and only detected by seismic stations >400 km away (Global Volcanism Program, 2001). In 1969, distant (>1,000 km) seismic and hydrophone detections of explosions placed renewed activity very near Ahyi (Norris & Hart, 1970), though discolored water was noted at a greater distance, roughly between Ahyi and Supply Reef. This activity was described as being very similar to recordings in 1967 from the same region (*Norris & Hart*, 1970; *Norris & Johnson*, 1969). Additionally, a fishing boat noted shocks and upwelling water containing sulfur near Ahyi in 1979 (*Global Volcanism Program*, 1979). During a regional survey of the submarine volcanoes of the Mariana Arc in 2003, Ahyi was found to be hydrothermally active (Baker et al., 2008; Resing et al., 2009).

3. Eruption Chronology

The 2014 Ahyi eruption began on 23 April at 20:35 UTC with ~2 hr of long duration signals ("sustained events") comprising impulsive events up to a few seconds long each that occurred at a high rate (several per minute; Figures 3 and 4d and Table 1). The first two sustained events lasted 3 and 1.6 min each. These were followed by a burst of activity between 21:53 and 22:24, which can be broken into five pulses of 2.4- to 7.5-min duration each. The last of the initial bursts of activity occurred from 21:59–22:35, broken into two pulses of 31.4- and 3-min duration. In the 25 min between the two long bursts, only a few small impulsive events occurred. Another lull in activity lasting ~1.5 hr began at 22:35 during which the only activity comprised several weak events and a small group of four stronger events and a few weak ones.

At 00:05 on 24 April, the short, impulsive events that were characteristic of the majority of the Ahyi eruption began (Figure 3 and Table 1). These impulsive events were typically observed as single events of up to a few seconds duration (Figure 4a), but they occasionally occurred in clusters of several events within about a minute (Figures 4b and 4c). The average event rate throughout the main eruptive period was ~25 events per hour (Figure 3), which remained remarkably steady through most of the eruption.

The U.S. Geological Survey (USGS) first noted converted T-phases from the eruptive activity on the CNMI seismic network (e.g., Figure 5) during the 24 April daily CNMI data check, but at that time the source could only be determined as north of Pagan Island. Follow-up with the Comprehensive Test-Ban Treaty Organization (CTBTO) constrained the source as near FdP based on back azimuths of detections by the Wake Island hydrophone arrays. On 25 April, as the impulsive events continued, the USGS raised the volcano aviation color code/alert level for Ahyi from Unassigned to Yellow/Advisory, indicating the potential dangers in the area.

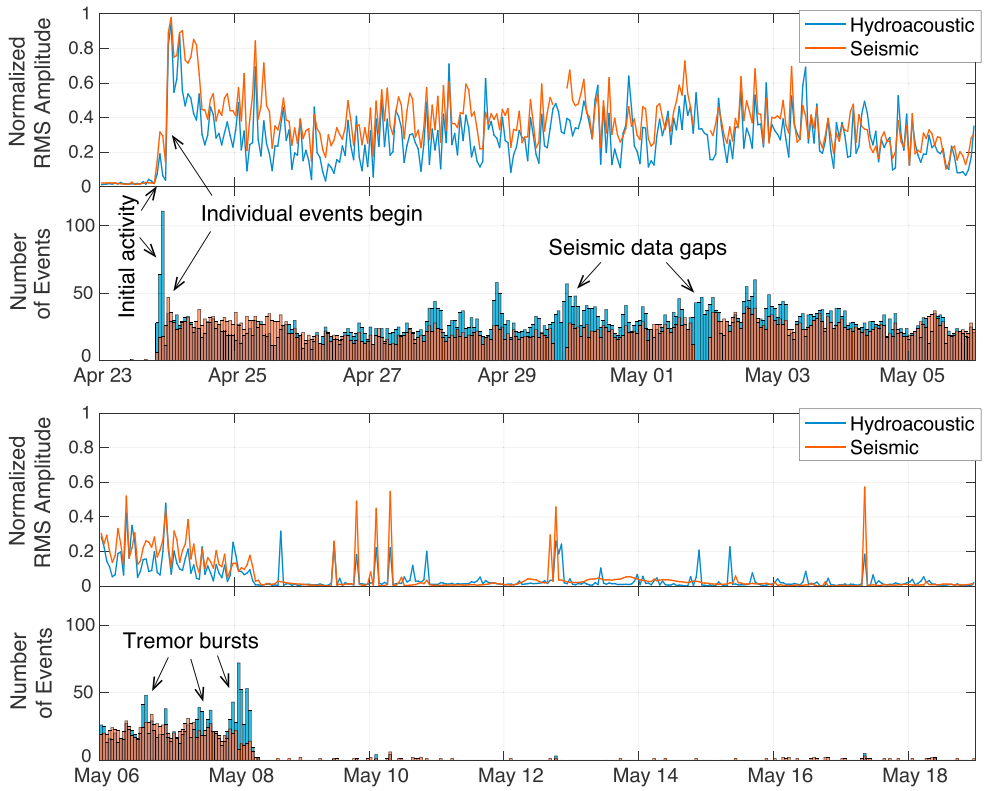

Figure 3. Normalized root-mean-square (RMS) amplitude (top) and event histogram (bottom) of seismic (red, PGNK) and hydroacoustic (blue, H11S1) data for 23 April to 18 May 2014. Data are corrected for travel times to stations (3 min for seismic, 25.3 min for hydroacoustic) and plotted in UTC at Ahyi. RMS amplitude was calculated in 1-hr, nonoverlapping windows. Hydrophone data were filtered between 4 and 70 Hz and seismic data between 3 and 12 Hz. Event counts are in 1-hr bins. RMS spikes that only occur in either the seismic or hydroacoustic data but not the other are typically the result of regional earthquakes or regional T-phases, respectively. Spikes in the hydroacoustic event counts at the beginning and end of the eruption are the result of sustained events that could not be detected by the short-term average/long-term average (STA/LTA) detector used on the seismic data.

On 6 May at 15:37, sustained events began to appear (Figure 3 and Table 1) and were observed until the end of the main eruptive period 2 days later. Most of these events occurred within four main periods: 6 May, 15:37–16:42; 6 May, 23:01–23:44; 7 May, 10:50–12:39; and 7 May, 22:30 to 8 May, 06:10. The sustained events were broadband (Figures 4e and 4f) and mostly continuous with very few strong impulsive events occurring simultaneously. Each sustained event lasted from tens of seconds to several minutes.

The main eruptive period ended at 06:10 on 8 May, although sporadic impulsive events and event clusters were observed until 18 May. After a week and a half of no activity, the USGS lowered the aviation color code/alert level back to Unassigned on 29 May.

4. Seismoacoustic Data & Methods

4.1. CNMI Seismic Networks

The USGS monitors the volcanoes in the Mariana region and operates a network of seismometers in the CNMI. At the time of the Ahyi eruption, the network comprised 14 stations distributed from north to south on the islands of Pagan (five stations, ~270 km away), Sarigan (one, ~420 km), Anatahan (four, ~460 km), and Saipan (four, ~580 km) as shown in Figure 1. The seismic stations were Guralp 6TD three-component broadband seismometers recording at 50 samples per second. Stations on each of the islands recorded signals from the Ahyi eruption (Figure 5). Based on arrival time delays across the network, these signals are converted T-phases that traveled most of their path through the water before being converted into seismic waves near the sensors. The signals also lack energy below 2–3 Hz, which is typical for waves propagating through the SOFAR channel (e.g., Okal, 2001). Signals from the Ahyi eruption were also detected by seismic stations

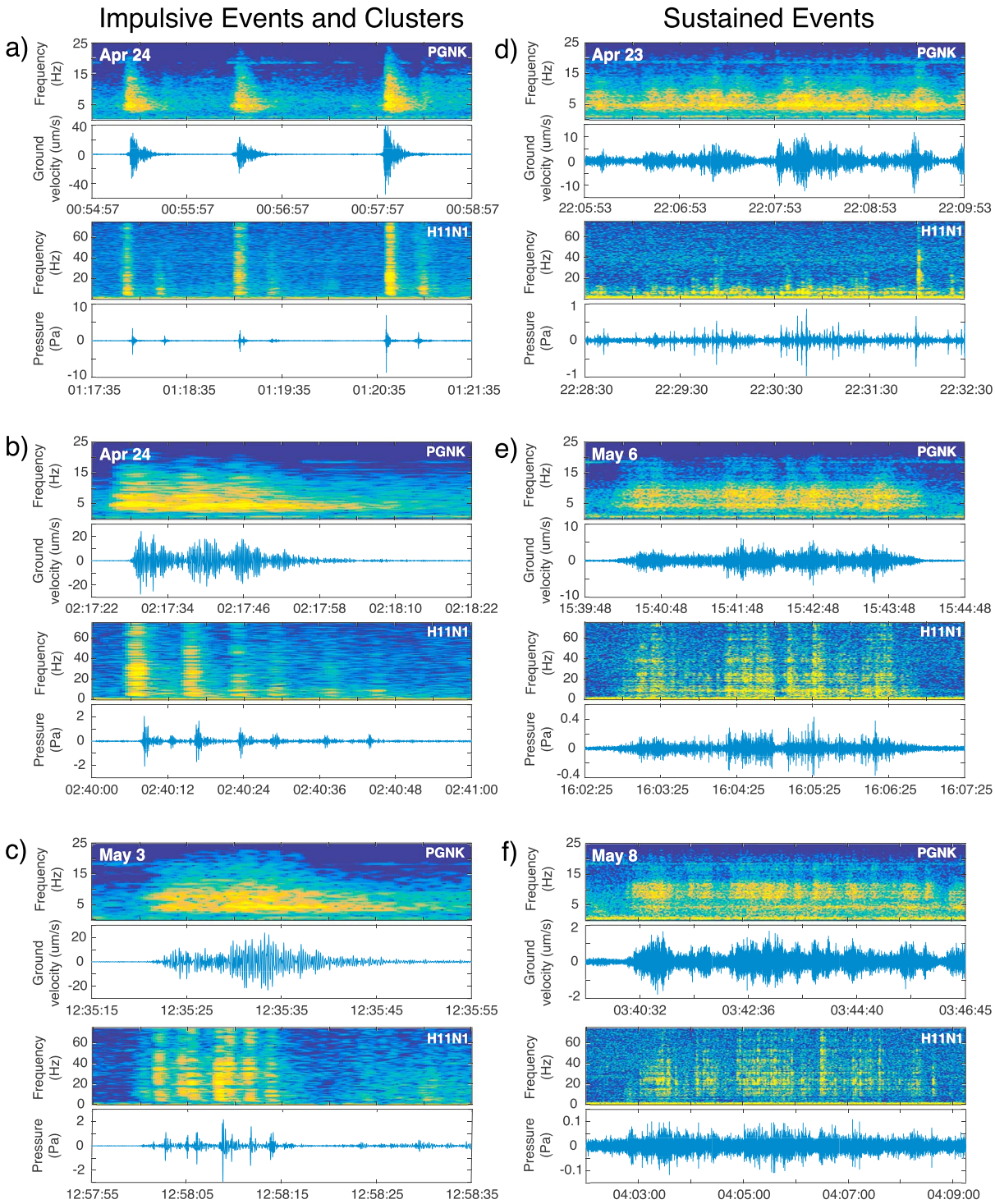

Figure 4. Types of geophysical activity recorded during the Ahyi eruption: (a) individual impulsive events, (b and c) clusters of impulsive events, (d) initial sustained event, and (e and f) sustained events during the last ~1.5 days of the eruption. Spectrograms and waveforms are from the PGNK seismometer (top) and H11N1 hydrophone (bottom). Waveforms are filtered between 3 and 12 Hz for seismic data and between 2 and 15 Hz for hydroacoustic data. Multipath arrivals are visible ~20 s after some of the hydrophone signals. Times are given in UTC at the receiver.

Table 1
Chronology of Major Events During the 2014 Eruption at Ahyi Seamount

Date and Time (UTC)	Description of event
23 April, 20:35	Heightened seismic/hydroacoustic activity begins
23 April, 20:35-22:35	Initial activity comprising groups of impulsive events and weak tremor
24 April, 00:05	Single impulsive events begin (with occasional event clusters)
24 April, 18:54	*USGS first notes seismic activity*
24–25 April 24	*NOAA coral reef expedition near Asuncion Island*
25 April	*Volcano aviation color code/alert level raised from Unassigned to Yellow/Advisory*
26 April	*NOAA coral reef expedition near Farallon de Pájaros*
27 April to 8 May	*NOAA coral reef expedition near the Maug Islands*
6 May, 15:37	Sporadic tremor bursts begin, primarily in four main periods
8 May, 06:10	Heightened seismic/hydroacoustic activity ends
8–18 May	A few sporadic events and event clusters occur
14–18 May	*NOAA bathymetric mapping and hydrothermal plume survey*
29 May	*Volcano aviation color code/alert level returned to Unassigned*

Note. Italics indicate nongeophysical events. USGS = U.S. Geological Survey; NOAA = National Oceanic and Atmospheric Administration.

on Guam (~770 km south) and Chichijima Island, Japan (~800 km north). These detections, particularly the latter, helped to constrain the source location of the activity while the eruption was ongoing. However, neither of these distant stations is used in this analysis. In this study, seismic data are band-pass filtered from 3–12 Hz, which includes the primary frequency range of recorded activity. This frequency range also largely avoids local, long-period events (<3 Hz) associated with concurrent, persistent, low-level eruptive activity at Pagan volcano (Lyons et al., 2016) or surf noise (Lyons et al., 2014).

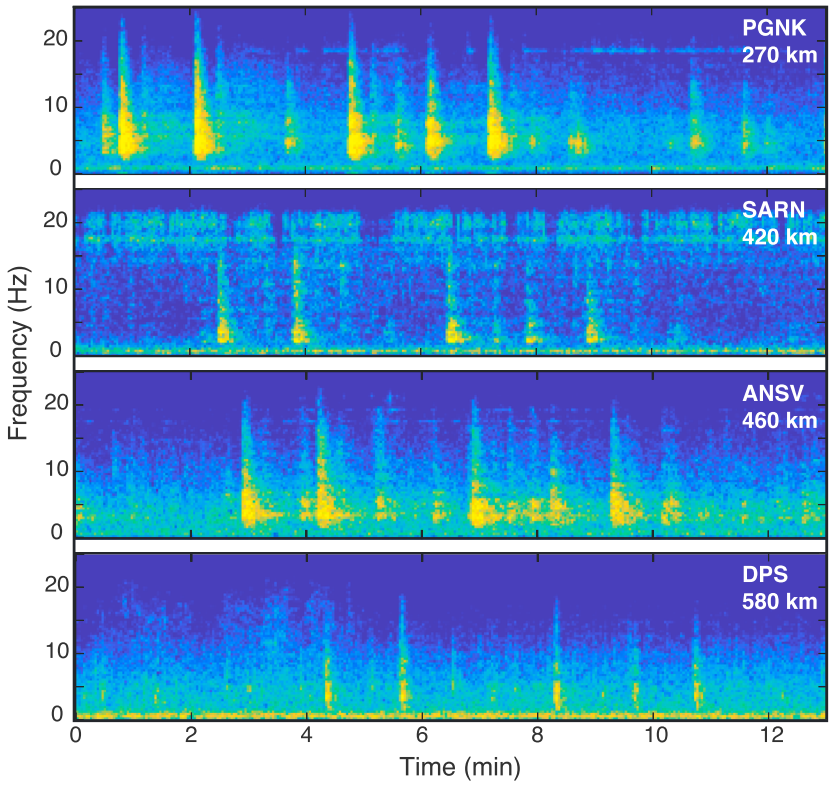

Figure 5. Spectrograms from one seismic station on each island in the Northern Mariana Islands network starting at 00:07:30 UTC on 24 April 2014. The lack of energy below ~3 Hz and the relative arrival time delays are consistent with converted T-phases, which propagate through the water for most of their path.

Station PGNK, on the southwestern part of Pagan Island (Figure 1), had the best recordings of the Ahyi activity and was used for single-station analyses. The slope of the seafloor within the SOFAR channel (approximated between 700- and 1,200-m depth) along the path between PGNK and Ahyi is ~25°. Although still less than the steep slopes of >50° desired for the best conversions (Talandier & Okal, 1998), this average slope is better than the gentler slopes of shield volcanoes and is likely the reason for the relatively efficient conversions on PGNK. Additionally, this slope measurement is averaged over a length of ~2 km and, thus, does not consider smaller areas of steeper slopes along this path or others where the hydroacoustic-seismic conversion may be happening.

4.1.1. STA/LTA Seismic Event Detection

An event catalog was generated using a standard short-term-average/long-term-average (STA/LTA) detector on seismic station PGNK. There were 7,881 events identified between the start of activity on 23 April and the last identified signal on 17 May (Figure 3). Of these, 7,815 occurred during the main eruptive period, and most are likely signals from Ahyi based on the following analyses of this study. During the main eruptive period, there were 6,616 events detected on Sarigan Island (station SARN), 6,170 on Anatahan Island (station ANSV), and 3,802 on Saipan Island (station DPS). However, on each station, the number of detections from the Ahyi eruption is expected to be lower than the total number of detections because the STA/LTA detector does not distinguish the source of the detections.

4.2. CNMI Infrasound Arrays

Infrasound arrays are also operated as part of the CNMI monitoring network. At the time of the eruption, there were four arrays in operation, two on Pagan Island (PGNW and PGBF, Figure 1) and one each on the islands of Sarigan and Saipan. Infrasound has previously been detected from underwater eruptions that produced subaerial clouds (e.g., Green et al., 2013). Even though there was no known subaerial activity during the Ahyi eruption, the limited surficial observations could have missed weak subaerial activity or acoustic signals could have been transmitted into the air due to a source at the shallow summit of Ahyi (e.g., Godin, 2007).

We analyzed data from the three northernmost arrays for coherent infrasound signals from the direction of Ahyi. This was done by least squares beamforming (Haney et al., 2018; Olson & Szuberla, 2005) continuous data from 23 April to 18 May using 60-s windows with 30-s overlap. Delay times between station pairs were determined through cross-correlation, with the root-mean-square (RMS) error required to be less than 0.05 s to ensure data consistency. When the maximum normalized cross-correlation value exceeded 0.5, we inverted for the slowness vector of a plane wave crossing the array and calculated the back azimuth and trace velocity of the signal. Signals were considered detections if they came from within +/−15° of the back azimuth from the center of the array to Ahyi and had a trace velocity between 250 and 450 m/s. Using these criteria and a filter band of 0.4–5 Hz, no coherent infrasound signals from Ahyi were detected on the three arrays. This is not a particularly surprising result because no volcanic clouds were detected in satellite data from the Ahyi eruption; however, with the relatively shallow depth to the summit of Ahyi, it is possible that future eruptions could generate subaerial clouds and produce detectable infrasound.

4.3. IMS Hydroacoustic Arrays

The CTBTO operates several hydrophone arrays as part of its International Monitoring System (IMS). The nearest arrays to Ahyi are those located north and south of Wake Island (H11 on Figure 1), ~2,250 km to the east. Each array consists of a triad of hydrophones recording at 250 samples per second. At the time of the eruption, detections on these arrays were critical for constraining the source of the hydroacoustic signals as being near Ahyi. Additionally, Metz and Grevemeyer (2018) examined the energy budgets and propagation of the Ahyi eruption signals at the Wake Island hydrophones. Two IMS hydrophone triads in the Juan Fernandez Islands, Chile (H03 north and south), also recorded a small percentage of the Ahyi events nearly 15,500 km across the Pacific Ocean, but those observations are not described here in detail. Metz et al. (2016) found similar long-distance detections of an eruption of Monowai Seamount. For our study, the H11S2 and H11N1 hydrophones were chosen as the best stations for single-station analyses.

4.3.1. Coherence Detector

We first applied the same coherence-based detector as used for the infrasound analysis to the hydroacoustic data from the Wake Island arrays. The coherence detector was applied to data from both the H11N and H11S arrays independently from 23 April to 20 May. We used nonoverlapping time windows of 15 s with data

filtered between 2 and 15 Hz. A minimum correlation value of 0.4 was required to make a detection. Multipath arrivals were often noted ~20 s after the main signals, usually with back azimuths that differed by −0.8° to −1° from the main arrivals. The stronger of these secondary arrivals also triggered the coherence detector but were largely removed from the detection list based on their back azimuths. During the main eruptive period, coherent detections were made for 9,554 windows with back azimuths between −80.6° and −81.3° on the H11S array and for 8,729 windows with back azimuths between −84.7° and −84° on the H11N array. Detections were made on both arrays for 6,246 of these windows. The average back azimuth and standard deviation for these detections was −80.97° ± 0.15° for H11S and −84.38° ± 0.13° for H11N, which agree well with the measured back azimuths to Ahyi of −81.1° and −84.3°, respectively. The largest variation of the back azimuths appears to be related to semidiurnal tides (see supporting information Text S1 and Figure S1). Because detections are made for the time windows analyzed rather than for each coherent signal, the number of coherence detections does not directly correspond to the number of events. Periods of tremor that were sustained for >15 s can result in multiple detections as can impulsive events that occur on the border between windows, while windows with multiple events will only count once. Thus, the number of hydroacoustic window detections is not directly comparable to the seismic STA/LTA detections.

4.4. Characteristics of Seismic and Hydroacoustic Events

Both the seismic and hydroacoustic data were analyzed for highly similar, or repeating, events. Highly similar events are assumed to have similar source mechanisms and locations, providing information about possible interrelations of events. Detections from the initial catalogs described in sections 3.1.1 and 3.2.1 were cross-correlated to look for event families. The PGNK events were first cross-correlated with an 11-s window to better align onsets, then were cross-correlated again using a 6-s window that included most of the event duration. A correlation cutoff of 0.6 resulted in 348 families with 243 events not correlating above this threshold. The largest family contained 5,147 events, ~66% of the total number of events. The stacked waveforms of events for each of the four largest families all correlated with each other above 0.66, and the stack of the largest family correlated with each of the other three above 0.8. Using a stricter correlation threshold of 0.8 resulted in three families with over 250 events each, with the largest family having 464 events.

The H11 coherence detections were also cross-correlated. Because the coherence detection times are given for the window rather than the coherent signal itself, the detections were first cross-correlated using the 15-s coherence detection window to align the signals and adjust the onset times. After the detections were aligned, they were cross-correlated using a 1.25-s window containing most of the event waveforms. Overall, the hydroacoustic detections did not correlate as well as the seismic detections on PGNK. One possible explanation for this is that the acoustic-seismic conversion may be causing the waveforms to become more uniform, for example, by filtering out higher frequencies that may be less similar from event to event. Using a correlation threshold of 0.5, the events grouped into 284 and 83 families on H11N1 and H11S2, respectively, with 26 and 4 events, respectively, not correlating above the threshold. On H11N1, the two dominant families included 4,506 and 2,476 detections, combining for 80% of the total number of detections. The stacked waveforms of these two clusters correlate at 0.85. The H11S2 detections did not correlate as well with three dominant families of 5,702, 1,446, and 1,176 detections for a combined total of 87% of the detections. The stacked waveforms of the three dominant families all correlate above 0.63 with the two largest correlating above 0.8. Using the same 0.6 cutoff as the seismic data results in half or less of the detections being included in the main families with >1,000 detections, three on H11N1 and two on H11S2. Further increasing the threshold to 0.8 resulted in no families with more than 250 events on either H11N or H11S, with the largest families having 211 and 244 events, respectively.

We also measured the maximum amplitude and average frequency of the detections to more fully characterize the events. The maximum amplitude was determined from an envelope of the event waveform. To calculate the average frequency, we first took the Fourier transform of the event waveform and calculated the power spectral density. The average frequency was then determined by normalizing the inner product of the power spectral density and the frequency vectors. The instrument response was removed before both of these measurements were made.

Given the large number of events, these parameters were each then averaged over 3-hr, nonoverlapping windows to look for trends over the duration of the eruption (Figure 6). The amplitudes of the detections started small but quickly increased to the largest amplitudes on 24 April. After a few hours, the

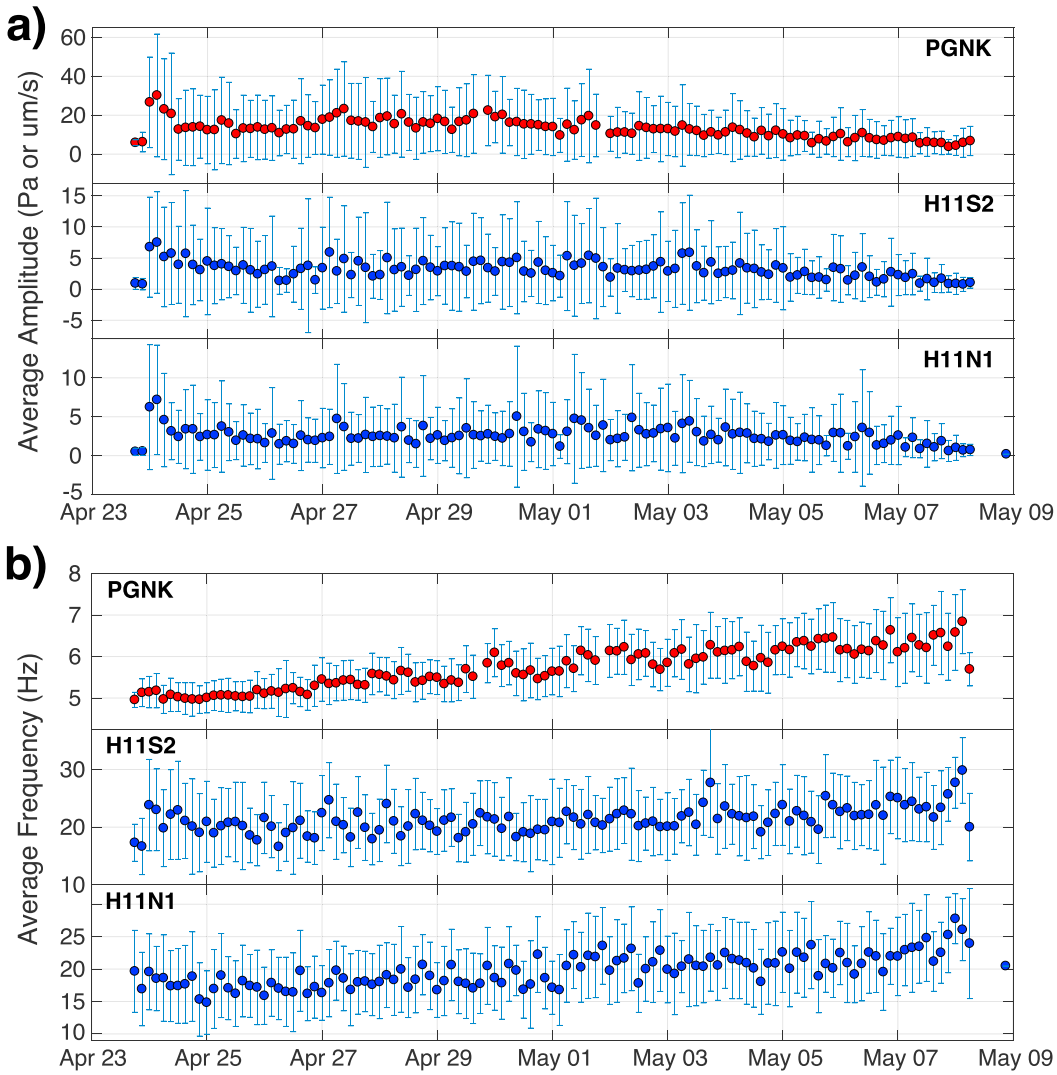

Figure 6. Plots showing the (a) amplitude and (b) average frequency of the detections over the duration of the Ahyi eruption 2014. Each circle represents the average of detections in a 3-hr bin with error bars indicating the standard deviation of values in each bin. Red and blue denote seismic and hydroacoustic detections, respectively, with the stations labeled.

amplitudes decreased then held steady before starting to rise again around 29 April. By 1 May, the amplitudes started to decrease again and continued to do so until the end of the main eruptive period on 8 May. The average frequencies increased relatively steadily over time, with the trend clearest in the seismic recordings. However, both lower- and higher-frequency events were recorded throughout the duration of the eruption with lower-frequency events more common early in the eruption and higher-frequency events more common later in the eruption. The sharp increase in average frequency in the hydrophone data during the last ~1 day of the eruption is from detection windows of the sustained events that were not detected by the STA/LTA detector applied to the seismic data. The standard deviation of the average frequency also increased over time, though only in the seismic data. The larger events recorded by the hydrophones had higher average frequencies throughout the eruption, whereas the larger events in the seismic data started with lower frequencies (supporting information Figure S2). This increase in the variability of average frequencies in the seismic explains the increase in standard deviation. The increase in frequencies was also noted by Metz and Grevemeyer (2018).

No seismic body waves could be easily identified on the Pagan seismic network, so we used the similarity of the T-phases to look for weak seismic body waves. The highly similar T-phase waveforms were aligned and

stacked to reduce noise and strengthen the correlated signal. We aligned the 5,147 events in the main seismically recorded family on the T-phase arrival time determined from station PGNK. We then stacked windows of the displacement waveforms starting 200 s before the T-phase arrival times on stations PGNK and PGBF. The stack was averaged, resulting in a waveform that was representative of the average impulsive event (supporting information Figure S3). This procedure reduced the background noise to 0.2 nm on PGBF and 2 nm on PGNK. However, no seismic body waves were apparent above the noise at either station. Using the lower background noise level as the maximum amplitude of a hypothetical seismic body wave, we can estimate a maximum magnitude (M_L) using the following relation:

$$M_L = \log10(A) + 2.56\ \log10(D) - 1.67,$$

where A is the displacement in micrometers and D is the distance in kilometers (Bullen & Bolt, 1985). With a distance of 267 km to station PGBF, we find that a hypothetical earthquake would need to have a magnitude of approximately 1 to have seismic body waves above noise level.

5. Near-Field Observations and Repeat Bathymetry

In addition to the distant geophysical observations, there were also some proximal observations made of the eruptive activity by several oceanographic expeditions conducting research on ships in the area (*Global Volcanism Program*, 2014). From 24–26 April, a coral reef monitoring expedition was working in the northern CNMI on the NOAA ship Hi'ialakai (HA1401-Leg3). Scuba divers first noted hearing underwater explosions on 24–25 April while they were near Asuncion Island (~90 km SE of Ahyi; Figure 2). When the expedition moved to FdP on 26 April (18 km NW of Ahyi), the explosions were heard even louder by the divers. They described the sounds as like "bombs exploding with the concussion felt through your body." One particularly large explosion reverberated through the hull of the ship, and the crew on board were concerned that there was a problem with the ship until the divers relayed that they were also hearing and feeling the explosions underwater. In addition to the explosions, the divers also noted mats of yellow-orange bubbles on the ocean surface stretching for ~7–9 m along the SE shoreline of FdP (on the side of the island facing Ahyi, Figure 2). It is unknown whether these were related to the eruption, but they are consistent with previous reports of surficial sulfur at Ahyi (e.g., Global Volcanism Program, 1979). The ship passed by Ahyi on the way to and from FdP, in the early morning and the evening, respectively, but did not observe any activity at the surface. Explosions continued to be heard during dives at Maug Islands (~50 km SE of Ahyi) that started on 28 April.

During the following expedition on the Hi'ialakai (HA1401-Leg4), the ship was working at Maug Islands from 12–18 May (after the main eruptive period had ended) and conducted several water column conductivity, temperature, and depth (CTD) casts around Ahyi that identified a hydrothermal plume coming from the seamount. Buck et al. (2018) describe the result of the CTD casts taken on 14 May 2014. They found that dissolved hydrogen was elevated up to 12.5 nmol/L (background ~2 nmol/L) on the west side of Ahyi, and methane was elevated up to 6 nmol/L (background ~2 nmol/L). Bathymetric data collected with the Hi'ialakai's EM300 multibeam sonar system in a single swath over the summit of Ahyi on May 14 showed significant depth changes compared to 2003. Together, these near-field observations confirmed that Ahyi was indeed the source of the eruption. This partial resurvey was later supplemented by a more complete bathymetric resurvey with an EM122 sonar system in December 2014 on the expedition RR1413 of R/V *Revelle* (Figure 7b; Moyer & Chadwick, 2017).

The posteruption bathymetric surveys were compared to a preeruption survey collected in 2003 during expedition TN153 on R/V *Thompson* using its EM300 sonar system (Figure 7a). Depth changes were determined by gridding the bathymetric data from the two surveys at 30-m resolution and then subtracting one grid from the other to create a grid of depth differences following the methods of Wright et al. (2008) and Chadwick et al. (2008). Previous studies have shown that depth changes between global positioning system (GPS)-navigated bathymetric surveys are significant above a threshold of ±10 m. However, not all depth changes above this threshold are real, but false positives can be eliminated by comparing with visual ground truth data from submersibles and/or determining whether they make geologic sense, based on their location and morphology. The areas of change we interpret to be real are outlined in blue and red in Figure 7c. In the following discussion, "positive depth changes" are where the seafloor became shallower due to

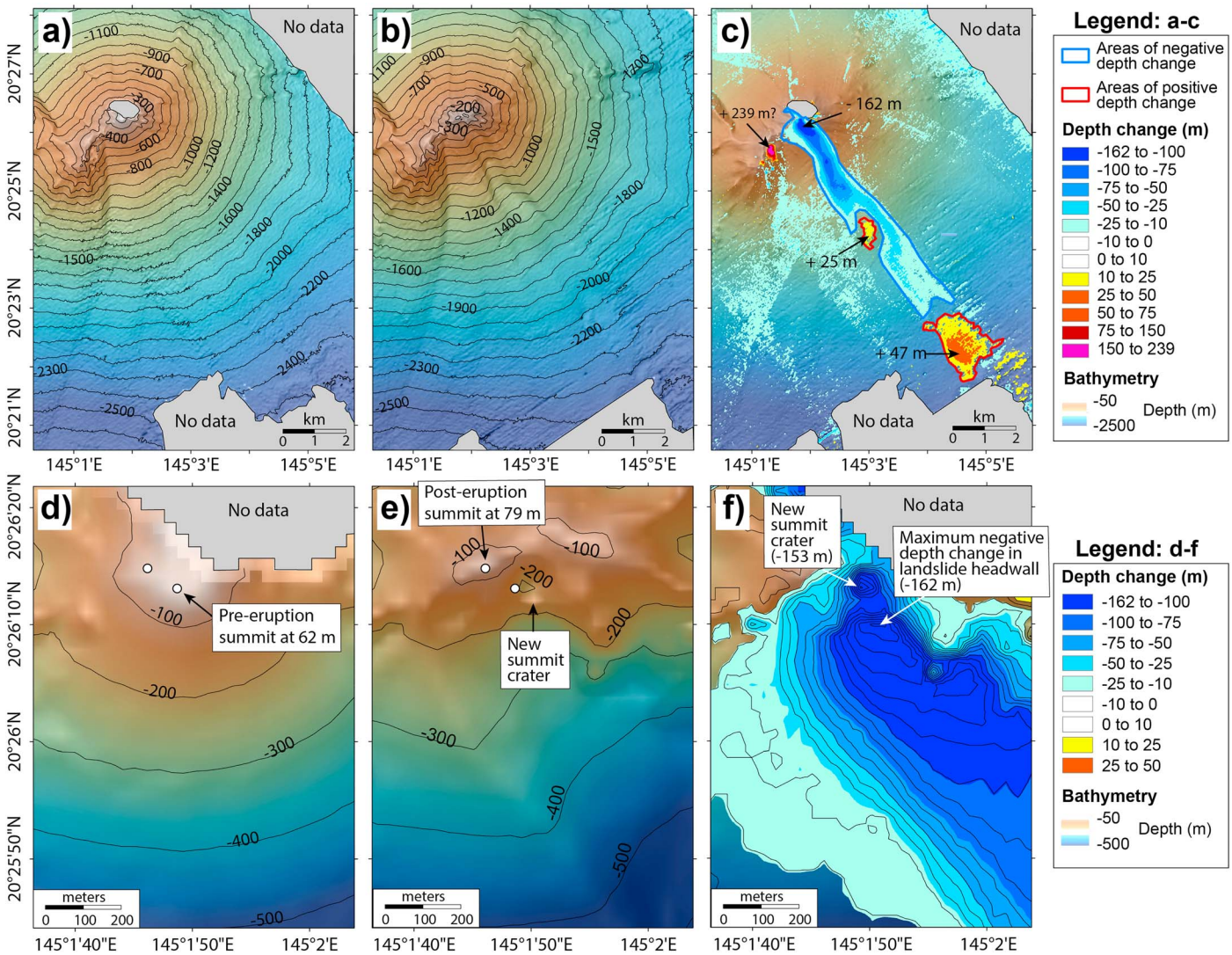

Figure 7. Bathymetric maps of Ahyi Seamount. Areas with no data coverage are gray. (a) Preeruption map from a survey in 2003 (cruise TN153 of R/V *Thompson*). Contour interval is 100 m. (b) Posteruption map from a survey in December 2014 (cruise RR1413 of R/V *Revelle*). (c) Depth changes between the 2003 and 2014 surveys (see color scale in legend) overlain on bathymetry from 2014. Blue and red outlines delineate areas of negative and positive depth changes, respectively, that are interpreted to be real and are used in volume calculations. Surrounding areas of apparent depth change (areas of light blue on flanks, and red area labeled "+239?") are considered noise and are ignored. Numbers with arrows indicate maximum depth change values within specific areas discussed in the text. (d) Preeruption map near summit. (e) Posteruption map near summit. (f) Depth changes near the summit (colors and 10-m contours) with new crater and landslide headwall labeled.

deposition of new material, and "negative depth changes" are where the seafloor became deeper due to removal of material.

The depth changes between the preeruption and posteruption surveys show the likely morphologic effects of the 2014 eruption (Figures 7c and 7f), though the exact timing is not known. The shallowest point of the seamount dropped by nearly 20 m from 60-m depth in 2003 to 79-m depth in 2014 and changed location. The posteruption surveys showed that a new crater had formed near the previous summit (located at 20°26.22′ N, 145°01.82′E; Figures 7d–7f) that is over 100-m deep from its north rim and 50-m deep from its south rim. The depth change at the center of the crater was −153 m (from −64-m depth in 2003 to −218-m depth in 2014). Most strikingly, a new landslide chute descended the southeast side of the volcano from the summit to at least 2,500-m depth. The landslide chute is about 9 km long and 0.6–1.1 km wide. Negative depth changes extend for ~7 km from the summit, and the upper half of the chute nearest the summit had the largest depth changes, where up to 162 m of material was removed from the head of the landslide. Downslope

Table 2
Thicknesses, Areas, and Volumes of Depth Changes at Ahyi Seamount from 2003 to 2014

Location description	Mean depth change (m)	Maximum depth change (m)	Area of depth change ($\times 10^6$ m^2)	Volume of depth change ($\times 10^6$ m^3)
#1—Positive depth change SW of summit (questionable)	82	239	0.17	13.90
#2—Negative depth change in chute	−32	−162	6.60	−211.23
#3—Positive depth change in midchute	12	25	0.29	3.38
#4—Positive depth change in lower chute	19	47	2.20	42.08
Positive totals (excluding #1 at summit)			2.49	45.46
Negative totals			6.60	−211.23
Net volume of depth change (positive − negative totals)				−165.77

of the chute is an area of positive depth change, up to 47 m, presumably deposits of landslide material that were moved downslope (Figure 7c). A second area of positive depth change, up to 25 m, is in the middle of the landslide chute (Figure 7c), surrounded by areas of negative depth change. This suggests that there were multiple landslide events because the smaller, midslope materials were deposited within the landslide chute after it had already formed.

A third area of positive depth change, up to 239 m, is located near the summit southwest of the new crater along a ridgeline; however, we doubt that it is real. This third area of depth change makes less sense geologically because it is located offset from the summit and the apparent eruptive vent, and in an area of steep slopes where it is easier to create large false depth differences from difficult navigation or poor data. While we cannot dismiss it entirely, we do not include it in the discussion that follows. Additional ground truth visual observations would be needed to determine if it is real (e.g., new deposits from an eruption) or not.

The total volume of negative depth change is -211×10^6 m^3 (Table 2), mostly a reflection of the amount of material moved from near the summit of Ahyi to its lower slopes, creating the landslide chute, but also including changes at the summit crater. However, the volume of positive depth change in the two areas within the chute totals 45×10^6 m^3, which is only 22% of the volume of negative change. This suggests that the area resurveyed in 2014 (which is limited) did not include all the landslide deposits and that there may be other areas of positive depth change farther downslope and/or that other materials were deposited perhaps more thinly and over a larger area, below the detection threshold of this technique (which is about 5–10 m).

One dive with the remotely operated vehicle (ROV) *Deep Discoverer* was made at Ahyi on 21–22 June 2016, during an expedition of the NOAA ship *Okeanos Explorer*. Dive EX1605L3-05 made a southwest to northeast traverse across the upper reaches of the 2014 landslide scar, south of the summit and crossing a depth range of 250–350 m (supporting information Figure S4a). The ROV dive track crossed areas where the 2003–2014 depth change varied from ~15 m in the southwest to ~150 m in the northeast (supporting information Figure S4b). The upper south flank of Ahyi was covered with coarse volcaniclastic debris (Figure 8a), probably from the 2014 eruption, that was clearly plagioclase-phyric (Figure 8b). Near the northeast end of the traverse, the volcaniclastic slope met nearly vertical outcrops of older massive jointed lava flows (Figure 8c). The shallowest part of the dive reached the headwall of the landslide (~250 m), downslope of the new crater where the ROV encountered white microbial mats indicative of diffuse hydrothermal venting (Figure 8d). Farther downslope from the crater were yellow microbial mats and coarser debris (Figure 8e). Southeast of the crater, the older massive lava cliffs exposed in the landslide headwall displayed dramatic columnar jointing (Figure 8f).

6. Interpretation and Discussion

6.1. Repeat Bathymetry

It is clear from the bathymetric data and other observations that an explosive eruption occurred at Ahyi in 2014 and was likely accompanied by landsliding. The previous volcano summit was replaced by a crater that is ~50–100 m deep, and a large landslide chute headed at the new crater formed on the SE slope. However, it is not clear from the repeat bathymetry how much material may have been erupted during the eruption. There are no large positive depth changes around the summit, except one thought to be an artifact and those in the depositional areas of the landslide chute. However, the detection threshold of the bathymetric

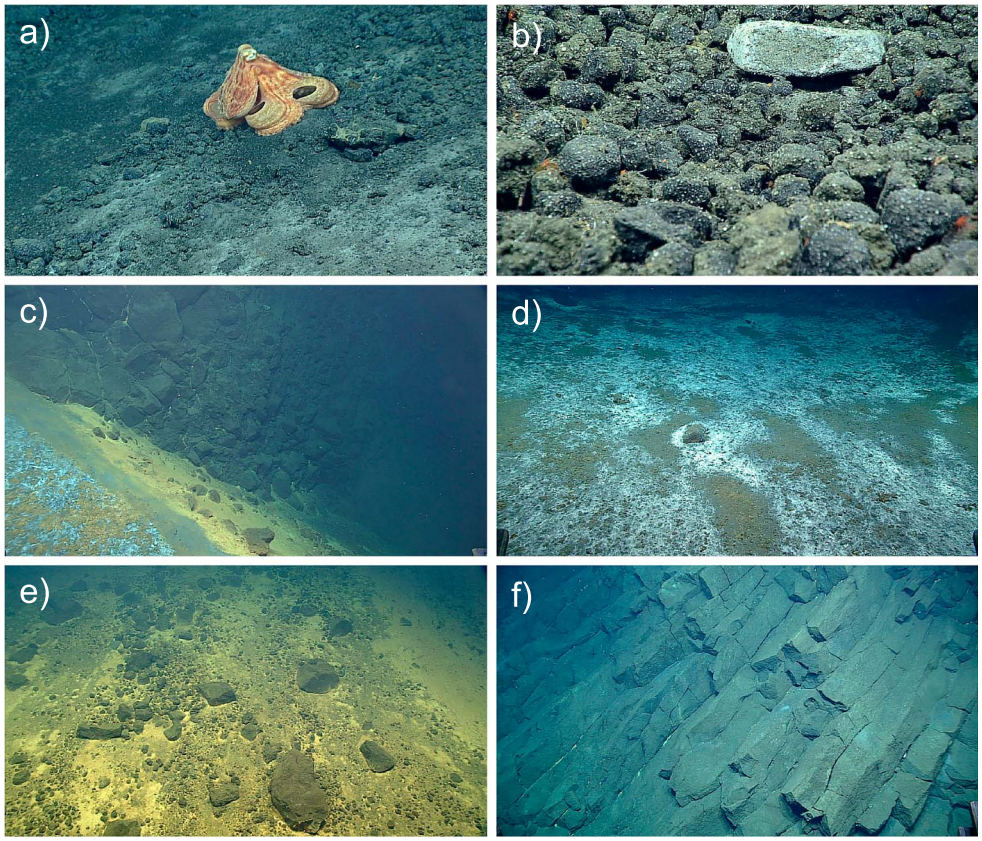

Figure 8. Images taken during *Deep Discoverer* remotely operated vehicle dive EX1605L3-05 (locations shown in supporting information Figure S4) in June 2016 across the head of the landslide scar (numbers following description are UTC time). (a) Octopus rests on coarse volcaniclastic debris near the SW end of the traverse (22:27:31). (b) Close-up of plagioclase-phyric volcaniclastic debris (23:23:07). (c) Area downslope of the new crater where the clastic-covered slope meets older massive lava outcrops (02:48:33). (d) Slope near the new crater covered in white microbial mats indicative of diffusing hydrothermal venting (01:46:48). (e) Area farther downslope with yellow mats and coarser debris (02:13:39). (f) Columnar joints in massive lava outcrops exposed by the landslide SE of the new crater (04:25:35).

comparison technique is 5–10 m (or more on steep slopes like at the summit of Ahyi), so it is likely there are eruption-related deposits not detected by this method. Another possible explanation is that much or all of the erupted material was fragmental and dispersed by ocean currents or was moved downslope by landsliding and distributed over a wide area at the base of the volcano. Either of these processes could result in relatively thin deposits that are either under the detection threshold or beyond the area that was re-surveyed. One other possibility is that the volume of new material that was erupted during the eruption was relatively small. Bathymetric and T-phase studies at the submarine volcano Kick-'em-Jenny in the Caribbean suggest that it has explosive eruptions with little deposition of new material (Allen et al., 2018), lending support to this idea.

6.2. Impulsive Events

The sharp character of the impulsive signals on the hydrophones suggests a shallow source (e.g., Bohnenstiehl et al., 2013; Dziak et al., 2005; Hanson et al., 2001), consistent with either a near-surface explosion or earthquake. However, without any seismic phase recordings or local instrumentation, distinguishing between the two is difficult. The spectra of these events are very broadband, reaching up to the ~100-Hz cutoff frequency of the hydrophones, which is more typical of explosions. Low-frequency dispersion, which has been observed as a characteristic of explosions (Talandier & Okal, 2016), is apparent on the distant H03 hydrophone recordings (supporting information Figure S5). Additionally, the reports by the NOAA divers of feeling and hearing "bomb-like" explosions during the occurrence of the impulsive events support an explosive source. However, shallow earthquakes could also potentially produce similar effects.

The changes in the signal character over the duration of the eruption can also be considered. As the eruption progressed, the average frequency of the event spectral content increased. The average event amplitude decreased throughout the eruption, with the largest events occurring in the first few days of activity. If the impulsive events were earthquakes, these changing characteristics could suggest that the earthquakes were getting smaller over time, leading to smaller amplitudes and more high-frequency content (or less low-frequency content) as reflected by the higher corner frequencies of the source spectra of smaller earthquakes. However, there does not appear to be any relation between amplitude and frequency of individual events (supporting information Figure S6). Alternatively, for an explosive source, lower amplitudes would indicate weaker explosions, but the change in frequency is not as straightforward to explain and could be the result of multiple factors. One possible explanation for the changing frequency content is a gradual changing of the summit or vent morphology as the crater was excavated. The crater excavation could also have caused a change in the average depth of the source relative to the surface above. Explosions occurring at shallower depths would allow more high-frequency energy to enter the water. Another possibility is that the gas content of the magma changed with time. Changes in frequency content due to explosive volcanic activity during an eruption have been reported previously by Thompson et al. (2002) and Haney et al. (2014) at Shishaldin and Pavlof volcanoes in Alaska, respectively.

While most of the impulsive events occurred individually, some were observed to occur in clusters of up to several events. The amplitude of the impulses within each cluster are variable. The ~20-s-delayed multipath arrivals are typically observed for all impulses in a cluster that are high enough amplitude for the multipath arrival to be above noise level (e.g., Figures 6b and 6c). For clusters lasting >20 s, multipath arrivals may sometimes be mixed in with the cluster events. The impulsive event clusters also became more common as the eruption progressed.

Similar clusters of impulsive events or arrivals have been observed elsewhere. *Green* et al. (2013) noted clusters of well-correlated impulsive events during the 2010 South Sarigan eruption that they interpreted as phreatomagmatic explosions associated with dome building. The South Sarigan event clusters were also recorded on local seismometers as converted T-phases only and, thus, interpreted as explosions (*Searcy*, 2013). In contrast, *Dziak* et al. (2012) observed local earthquakes at Axial Seamount in the northern Pacific Ocean on ocean-bottom hydrophones. They found that the earthquake recordings on the hydrophone comprised several impulsive-event-like arrivals, similar to the Ahyi event clusters. The various arrivals in the Axial earthquake signals were created by multiple acoustic phase reflections between the sea surface and seafloor. The Ahyi event clusters could potentially fit either of these interpretations. However, given the lack of seismic body waves recorded, an explosive source similar to that at South Sarigan seems the most reasonable.

Taking into consideration the available data and what is known about hydroacoustic signals, either an explosive or earthquake source is possible for the impulsive events. Given the similarity of the main families of individual events, it seems likely that the majority are either explosions or earthquakes rather than a mix of the two different sources. For the 2014 eruption of Ahyi, we feel the evidence favors an explosive source for the individual events and most, if not all, of the clusters. The seismic waveform stacking on station PGBF did not reveal any seismic body waves above the reduced noise level, meaning that if the individual events are earthquakes, they must be below magnitude 1. It seems implausible that such small earthquakes could produce T-phases detected on hydrophones across the Pacific Ocean over 15,500 km away. Furthermore, Metz and Grevemeyer (2018) suggest that earthquakes would need a minimum magnitude of 2.5 to be detected on the Wake Island hydrophones, though their analysis draws on tectonic earthquakes up to 80 km deep and does not consider earthquakes in the edifice that could produce signals directly into the SOFAR channel. While we interpret the recorded impulsive events as explosions, we cannot rule out the possibility of this eruption having earthquakes because small earthquakes could have gone undetected by the relatively distant (>250 km) sensors. This happened during the 2010 eruption of South Sarigan where a nearby seismometer (~10-km distant) recorded small precursory earthquakes (Searcy, 2013) that were not reported in analyses of distant IMS data (Green et al., 2013).

6.3. Sustained Events

Sustained events are defined here as signals that are nearly continuous over several tens of seconds to several minutes. Unlike impulsive events, they do not typically have a sharp onset. Two general interpretations of these signals are possible: (1) they are seismic tremor from sub-surface magma movement or high-rate

earthquakes or (2) they are tremor generated by eruptive activity. Sustained events occurred during the initial 2 hr of the eruption and during the last ~1.5 days of the main phase. The character of the sustained events in each of those two groups differed, suggesting that multiple processes were involved. However, it is also possible that the changes in character between sustained signals early in the eruption and those at the end may simply reflect the intervening changes in the eruptive crater morphology.

The first period with sustained events marked the beginning of the eruption and occurred for ~2 hr. These initial events were characterized by lower frequencies (<~20 Hz) and mostly comprised impulsive events. We interpret this activity as phreatomagmatic explosions that occurred as magma initially reached the surface and came into contact or mixed with seawater under the right conditions (e.g., Kokelaar, 1986; Wohletz, 1986), similar to the event clusters observed at the start of the South Sarigan eruption (Green et al., 2013). The lower frequencies typical of the initial sustained events are likely a result of relatively low level activity, with broader band energy observed for the occasional larger explosions. Bohnenstiehl et al. (2013) found low-frequency (1–20 Hz) tremor associated with the start of the 2009 eruption of Hunga Tonga-Hunga Ha'apai (HT-HH), Tonga Islands that they interpreted as magma moving up through a conduit and/or being erupted. However, in this case, the tremor continued for much longer, ~2.5 days, and was more continuous.

The second period of sustained events, in the form of tremor bursts, occurred during the final ~1.5 days (6–8 May) of the main eruption period in four main groups with occasional sporadic bursts at other times. These tremor bursts were broadband and comprise many small, very short, well-correlated events at rates of tens per minute. Each burst had a duration of up to several minutes. We interpret these tremor bursts as more sustained explosive activity, occurring after the vent had been fully opened.

6.4. Landsliding

The 2003 bathymetry shows that landslide events like the one(s) revealed in the 2014 survey have occurred before at Ahyi. For example, similar landslide chutes can be seen in the morphology of the cone on both the north and south flanks (Figure 7a), and the chute that likely formed in 2014 was carved into one of the pre-existing landslide scars. This is similar to what has been observed at other actively erupting submarine arc volcanoes, such as Monowai in the Kermadec Arc, NW Rota-1 in the Mariana Arc, and West Mata in the NE Lau Basin. At Monowai, which has a similar summit depth as Ahyi (<150 m), intermittent eruptive activity over many years has been interspersed with multiple landslides on different sectors of the volcano (Chadwick, Wright, et al., 2008; Watts et al., 2012; Wright et al., 2008). Similarly at NW Rota-1, low-level strombolian eruptive activity between 2003 and 2009 deposited volcaniclastic deposits on the upper southern slope of the volcano, which were then moved downslope in a major landslide in 2009 (Chadwick et al., 2008; Chadwick et al., 2012; Embley et al., 2006; Schnur et al., 2017). West Mata volcano was observed to be erupting continuously between 2008 and 2011 by direct ROV observations and remote hydrophone recordings (Dziak et al., 2015; Resing et al., 2011). Comparison of multiple bathymetric surveys of the volcano between 1996 and 2012 revealed areas of depth change from both continuous and discrete eruptive events and landslides (Clague et al., 2011; Embley et al., 2014), and hydrophone monitoring captured some of the landslide activity (Caplan-Auerbach et al., 2014). In all of these cases, the eruptive and landslide activity are linked to one another. Repeated deposition of fragmental volcaniclastic materials near the volcano summit eventually become oversteepened and gravitationally unstable. This leads to landsliding, usually in narrow chutes on individual sectors of the seamounts, to move that material to the lower slopes, possibly similar to processes documented at subaerial volcanoes (e.g., Waythomas et al., 2014).

There were likely one or more landslide events that formed the chute identified in the 2014 bathymetry, but none of the identified hydrophone or seismic signals from the Ahyi eruption appear to relate to landsliding. While multiple smaller landslides could have produced signals that were too weak or diffuse to propagate the long distance to the Wake Island arrays or to survive the hydroacoustic-to-seismic conversions at the CNMI seismic stations, one large landslide could potentially have produced detectable hydroacoustic signals. Wright et al. (2008) and Chadwick et al. (2012) describe hydroacoustic signals associated with sector collapses paired with large eruptions. However, neither of those signals are similar to anything recorded during the Ahyi eruption, and the bathymetric data do not show a comparable sector collapse of the seamount. Other studies have identified submarine landslide signals in hydroacoustic data (e.g., Caplan-Auerbach et al., 2001; Caplan-Auerbach et al., 2014; Drobiarz, 2017). Such signals are typically broadband, nonimpulsive, and last for tens of seconds or more. The sustained events recorded during the last 1.5 days of the Ahyi

eruption could potentially fit the description. However, the interference bands present in the sustained event signals are steady and similar to the interference bands of the impulsive events, suggesting that the source is stationary and likely near the source of the impulsive events (i.e., near the active vent).

Another possibility is that the landslide occurred outside the time frame of our data analysis, though still before the first bathymetric resurvey on 12–18 May. However, because seismoacoustic data were examined through late May, the landslide would have had to occur prior to the eruption onset on 23 April in that scenario. Given that landslides at submarine volcanoes typically occur along with eruptions, as described above, a landslide prior to the 2014 eruption seems unlikely, unless there was an undetected or unrecognized eruption between 2003 and 2014. While small landslides related to mass wasting may have occurred in the interval between eruptions, these would likely be below the detection threshold of repeated multibeam surveys (±10 m). The 2014 slide is relatively large and similar to ones documented as associated with eruptive activity at NW Rota-1, Monowai, and West Mata volcanoes. Thus, we interpret the Ahyi landslide as most likely occurring along with the 2014 eruption.

6.5. Summary and Discussion of the Eruption Interpretation

Pulling all of this information together, we can outline our interpretation the sequence of events during the 2014 Ahyi eruption. The eruption began on 23 April with an opening phase that produced both sustained and impulsive events. The sustained events are interpreted as phreatomagmatic explosions as the system was opening up. The opening phase was followed by a short ~90-min pause in activity. This pause is most notable for the cessation of the sustained events, which do not return when activity picks back up. The pause could be explained by a blocking of the conduit or a temporary pause in the driver (e.g., not enough magma pressure) or some combination of the two.

After the pause, the main phase of the eruption began and continued fairly steadily for 2 weeks. This phase was defined by thousands of impulsive events that were well correlated, indicating a similar source and location. A maximum source dimension can be approximated as one fourth the dominant wavelength (Geller & Mueller, 1980). In this case, the lowest average frequencies were ~5 Hz on the hydrophones, with a corresponding wavelength of ~300 m. Thus, the largest dimension of the explosion source area is approximated as 75 m, similar in size to the new summit crater. During this phase, we interpret that explosions occurred in the new summit crater, ejecting material and accounting for most or all of the −153-m depth change observed in the bathymetric data. Impulse clusters that occurred throughout the main phase were likely groups of crater explosions but could also be earthquakes produced by internal stress changes in the system. Sustained events in the last few days of the eruption may be more sustained explosive eruptions. However, these sustained events had different frequency spectra than those recorded during the opening phase. This could indicate a difference in source (e.g., gas-driven rather than phreatomagmatic explosions) or simply reflect the morphological changes in the edifice.

The eruption largely concluded at the end of the main phase. A few impulsive events and clusters occurred over the following ~1.5 weeks, as the eruption rapidly waned. Without a clearly associated signal, it is unclear when exactly the landslide(s) occurred. If one large landslide is responsible for the chute, it most likely happened near the end of the eruption once enough new fragmental eruptive deposits had built up. If the chute was formed by several small landslides, these may have occurred throughout much of the main phase.

Other submarine eruptions have followed similar sequences. Bohnenstiehl et al. (2013) examined regional hydrophone recordings of the 2009 HT-HH eruption, which also had a shallow submarine summit. Unlike the 2014 Ahyi eruption, they found that the HT-HH eruption was immediately preceded by earthquakes up to magnitude 4.8. However, the rest of the HT-HH eruption was quite similar to the Ahyi eruption. The ~2 hr of earthquakes were followed by a low-frequency tremor signal with occasional discrete events, similar to what was observed at the start of the Ahyi eruption. They describe impulsive, broadband signals (up to 125 Hz) from Surtseyan-type explosions that begin ~1.5 hr after the tremor onset. Given that the HT-HH eruption breached the sea surface, visual observations were able to confirm that explosive activity was occurring around the times that the impulsive events were detected, although the study did not match individual explosions with specific signals. The low-frequency tremor and explosions occurred for almost 3 days before the activity dropped off. Overall, this is much shorter than the Ahyi eruption. However, the sequence of events and the types of signals observed are very similar. Both eruptions

opened with low-frequency tremor interpreted as magma movement, which was followed by impulsive signals from likely explosions.

In contrast, some submarine arc volcanoes have different eruption styles. The deeper NW Rota-1 (517-m summit depth) and West Mata (1,174-m summit depth) volcanoes both tend to produce longer, low-level degassing explosion signals that last for up to a few minutes and that start and end rather abruptly (e.g., Chadwick, Cashman, et al., 2008; Dziak et al., 2015). The signals also tend to be widely broadband (up to ~100 Hz). Both of these volcanoes were reported to have long-lived eruptions: West Mata lasting for >2 years and NW Rota-1 going for >7 years. The 2014 Ahyi eruption was much shorter than these eruptions and was dominated by impulsive events. Only the tremor signals at the end were potentially produced by sustained, or degassing, eruptions. Both of the NW Rota-1 and West Mata eruptions also had landslides associated with them (e.g., *Caplan-Auerbach* et al., 2014; Chadwick et al., 2012), which was likely the case for the Ahyi eruption, too. Short impulsive signals have been recorded at West Mata as well as the broadband signals and were interpreted as magam bubble bursts (Dziak et al., 2015). These impulsive signals were fairly weak and only detected by a hydrophone very close to the active vent (<0.5 km), so it is unlikely that the impulsive Ahyi events recorded at Wake Island are related to similar magma bubble bursts.

6.6. Comparison of Hydroacoustic and Seismic Data

With both seismic and hydroacoustic recordings of the eruption, it is worthwhile to briefly comment on how they compare. Seismic stations that are optimized for recording T-phases, such as those of the CTBTO or the Polynesian Seismic Network, are sometimes used in lieu of hydrophones to detect hydroacoustic events as they are logistically easier and less expensive to install and maintain (e.g., Okal, 2001). Additionally, other nonoptimized seismic stations, such as those in the CNMI network, can also detect T-phases. Thus, understanding how T-phases may be recorded by the different instruments is important for identifying and characterizing the source. In the case of the Ahyi eruption, the seismic stations are distant enough that seismic body waves were not recorded, meaning that we are comparing only T-phases on a seismometer and hydrophone. It is important to note that this comparison, however, is with a nonoptimized seismometer located near a less-than-ideal submarine slope (<50°), so the following comments may not hold for dedicated T-phase stations that are optimized for detecting T-phases. On the other hand, for monitoring in volcanic arcs using pre-existing seismic networks that may not be ideal for detecting T-phases, such as in the CNMI, the following considerations are necessary.

Perhaps the most obvious difference is the duration of the T-phases on the hydrophone versus the seismic recordings (Figure 6). The hydrophone recordings maintain the shorter, sharper character of the impulsive events that is likely produced by the source. In comparison, the seismic recordings of the same events are more drawn out, lasting several seconds (Figure 6a), due to conversion and path processes (e.g., seismic scattering). This becomes an issue when trying to discriminate between closely spaced events. For example, the event clusters identified from the hydrophone records often appeared as single T-phases in the seismic recordings (Figure 4c). While the individual event peaks might be visible in the drawn out seismic signal, they might not be recognized as individual events.

The frequency content of the T-phases also varies between the two data types. The seismic recordings appear to have lost much of the higher-frequency (>~12 Hz) energy. The loss is likely from attenuation after the wave has already converted to a seismic signal, but some of the loss may come from the conversion itself. This loss of higher frequencies along with the duration effects can cause different types of signals in the hydrophone recordings to take on a similar character in the seismic recordings. This is noted in the different sustained events of the Ahyi eruption (Figures 6d–6f), which appear similar in the seismic recordings despite having clear differences in the hydrophone recordings.

Seismic stations, especially those located in areas of less efficient conversion, can be useful for the general monitoring of submarine volcanoes. During the Ahyi eruption, even though much of the character of the original signals was lost, the seismic station was still capable of recording all, or possibly even more, of the events produced by the eruption than the much more distant hydrophones. However, identifying the processes producing the signals, and thus understanding what the volcano is doing, likely requires hydrophones, more optimized seismic T-phase stations, or some other proximal ocean-based instruments (e.g., ocean-bottom seismometers).

7. Summary

Ahyi Seamount erupted in April–May 2014 for the first time in 13 years, but the eruption had little or no manifestation at the ocean surface. Detections by distant hydrophones and island-based seismometers allowed for a seismoacoustic characterization of the eruption. Repeat bathymetry of Ahyi obtained several years before and soon after the eruption along with a few direct observations made in the vicinity aided in confirming that Ahyi was the source of the eruption and in interpreting the geophysical signals. The main eruptive period lasted for about 2 weeks and was defined by up to about 8,000 impulsive signals that we interpret as phreatomagmatic explosions. The eruption began with ~2 hr of seismic activity interpreted as indicating shallow magma intrusion and reawakening of the system. Tremor signals, interpreted to be from more continuous explosive activity, were also produced during the last ~1.5 days of the main eruptive period. Sporadic explosions were observed for a further 10 days after the main eruptive period concluded. Repeat bathymetry identified a new summit crater, the likely location of the explosive eruption signals, and a large new landslide chute on the south side of the seamount. The landslide chute is inferred to be the result of multiple small landslides occurring during the eruption. It is difficult to quantify the volume of material erupted, but the available evidence suggest that the volume was relatively small. The seismoacoustic character of the eruption was more similar to other known shallow or at-surface submarine eruptions than to deeper (>500 m) eruptions.

Data

The seismic data used in this study are available from the IRIS Data Management Center (https://doi.org/10.7914/SN/MI). The hydroacoustic data can be obtained by contacting the CTBTO (https://www.ctbto.org/specials/vdec/). Bathymetry data from 2003 and 2014 are available from the NOAA National Centers for Environmental Information at https://www.ngdc.noaa.gov/ships/thomas_g_thompson/TN153_mb.html and https://www.ngdc.noaa.gov/ships/roger_revelle/RR1413_mb.html, respectively. The GISMO Waveform Suite and Correlation Toolbox (Thompson & Reyes, 2018) were extensively used and are available for download on GitHub. Bathymetry for map in Figure 1 retrieved from the Global Multi-Resolution Topography (GMRT) Synthesis database (Ryan et al., 2009).

Acknowledgments
We would like to thank Del Bohnenstiehl for helpful discussion and comments on the manuscript. We also thank Cheryl Searcy, Jackie Caplan-Auerbach, and an anonymous reviewer for their helpful and thorough reviews of the manuscript. Special thanks to Mark Prior from the CTBTO for sharing the real-time Wake Island detections in 2014 during the eruption. Support for field work during the NOAA ship Hi'ialakai expedition in May 2014 and the Submarine Ring of Fire 2014-Ironman cruise in December 2014 on R/V *Revelle* was provided by the NOAA Ocean Exploration and Research (OER) Program (Grant OE-FY14-71), the National Science Foundation (Award OCE-1155756, Craig Moyer, PI), and NOAA's Pacific Marine Environmental Laboratory. NOAA-OER also supported the Okeanos Explorer expeditions in the Mariana region in 2016. G. Tepp was supported by the USGS Mendenhall Fellowship Program. PMEL Contribution 4794. Any use of trade, firm, or product names is for descriptive purposes only and does not imply endorsement by the U.S. Government.

References

Allen, R. W., Berry, C., Henstock, T. J., Collier, J. S., Dondin, F. J.-Y., Rietbrock, A., et al. (2018). 30 years in the life of an active submarine volcano: A time-lapse bathymetry study of the Kick-'em-Jenny volcano, Lesser Antilles. *Geochemistry, Geophysics, Geosystems*, *19*, 715–731. https://doi.org/10.1002/2017GC007270

Baker, E. T., Embley, R. W., Walker, S. L., Resing, J. A., Lupton, J. E., Nakamura, K., et al. (2008). Hydrothermal activity and volcano distributions along the Mariana Arc. *Journal of Geophysical Research*, *113*, B08S09. https://doi.org/10.1029/2007JB005423

Bohnenstiehl, D. R., Dziak, R. P., Matsumoto, H., & Lau, T. K. A. (2013). Underwater acoustic records from the March 2009 eruption of Hunga Ha'apai-Hunga Tonga volcano in the Kingdom of Tonga. *Journal of Volcanology and Geothermal Research*, *249*, 12–24. https://doi.org/10.1016/j.jvolgeores.2012.08.014

Buck, N. J., Resing, J. A., Baker, E. T., & Lupton, J. E. (2018). Chemical fluxes from a recently erupted shallow submarine volcano on the Mariana Arc. *Geochemistry, Geophysics, Geosystems.*, *19*, 1660–1673. https://doi.org/10.1029/2018GC007470

Bullen, K. E., & Bolt, B. A. (1985). *An introduction to the theory of seismology*. Cambridge: Cambridge University press.

Caplan-Auerbach, J., Dziak, R. P., Bohnenstiehl, D. R., Chadwick, W. W. Jr., & Lau, T.-K. A. (2014). Hydroacoustic investigation of submarine landslides at West Mata volcano, Lau Basin. *Geophysical Research Letters*, *41*, 5927–5934. https://doi.org/10.1002/2014GL060964

Caplan-Auerbach, J., Fox, C. G., & Duennebier, F. K. (2001). Hydroacoustic detection of submarine landslides on Kilauea volcano. *Geophysical Research Letters*, *28*(9), 1811–1813. https://doi.org/10.1029/2000GL012545

Chadwick, W. W. Jr., Cashman, K. V., Embley, R. W., Matsumoto, H., Dziak, R. P., de Ronde, C. E. J., et al. (2008). Direct video and hydrophone observations of submarine explosive eruptions at NW Rota-1 Volcano, Mariana Arc. *Journal of Geophysical Research*, *113*, B08S10. https://doi.org/10.1029/2007JB005215

Chadwick, W. W. Jr., Dziak, R. P., Haxel, J. H., Embley, R. W., & Matsumoto, H. (2012). Submarine landslide triggered by volcanic eruption recorded by in-situ hydrophone. *Geology*, *40*(1), 51–54. https://doi.org/10.1130/G32495.1

Chadwick, W. W. Jr., Wright, I. C., Schwarz-Schampera, U., Hyvernaud, O., Reymond, D., & de Ronde, C. E. J. (2008). Cyclic eruptions and sector collapses at Monowai submarine volcano, Kermadec arc: 1998–2007. *Geochemistry, Geophysics, Geosystems*, *9*, Q10014. https://doi.org/10.11029/12008GC002113

Clague, D. A., Paduan, J. B., Caress, D. W., Thomas, H., Chadwick, W. W. Jr., & Merle, S. G. (2011). Volcanic morphology of West Mata Volcano, NE Lau Basin, based on high-resolution bathymetry and depth changes. *Geochemistry, Geophysics, Geosystems*, *12*, QOAF03. https://doi.org/10.1029/2011GC003791

Crisp, J. A. (1984). Rates of magma emplacement and volcanic output. *Journal of Volcanology and Geothermal Research*, *20*(3-4), 177–211. https://doi.org/10.1016/0377-0273(84)90039-8

Drobiarz, J. G., (2017) "Interpreting the dynamics of submarine landslides through hydroacoustic modeling, West Mata volcano, NE Lau Basin" WWU Masters Thesis Collection. 593.

Dziak, R. P., Bohnenstiehl, D. R., Baker, E. T., Matsumoto, H., Caplan-Auerbach, J., Embley, R. W., et al. (2015). Long-term explosive degassing and debris flow activity at West Mata submarine volcano. *Geophysical Research Letters*, *42*, 1480–1487. https://doi.org/10.1002/2014GL062603

Dziak, R. P., Haxel, J. H., Bohnenstiehl, D. R., Chadwick, W. W. Jr., Nooner, S. L., Fowler, M. J., et al. (2012). Seismic precursors and magma ascent before the April 2011 eruption at Axial Seamount. *Nature Geoscience*, *5*(7), 478–482. https://doi.org/10.1038/ngeo1490

Dziak, R. P., Park, M., Matsumoto, H., & Byun, S. K. (2005). Hydroacoustic records and a numerical model of the source mechanism from the first historical eruption of Anatahan Volcano, Mariana Islands. *Journal of Volcanology and Geothermal Research*, *146*(1-3), 86–101. https://doi.org/10.1016/j.jvolgeores.2004.12.009

Embley, R. W., Baker, E. T., Butterfield, D. A., Chadwick, W. W. Jr., Lupton, J. E., Resing, J. A., et al. (2007). Exploring the Submarine Ring of Fire: Mariana Arc—Western Pacific. *Oceanography*, *20*(4), 69–80.

Embley, R. W., Chadwick, W. W. Jr., Baker, E. T., Butterfield, D. A., Resing, J. A., de Ronde, C. E. J., et al. (2006). Long-term eruptive activity at a submarine arc volcano. *Nature*, *441*(7092), 494–497. https://doi.org/10.1038/nature04762

Embley, R. W., Merle, S. G., Baker, E. T., Rubin, K. H., Lupton, J. E., Resing, J. A., et al. (2014). Eruptive modes and hiatus of volcanism at West Mata seamount, NE Lau Basin: 1996-2012. *Geochemistry, Geophysics, Geosystems*, *15*, 4093–4115. https://doi.org/10.1002/2014GC005387

Embley, R. W., Tamura, Y., Merle, S. G., Sato, T., Ishizuka, O., Chadwick, W. W. Jr., et al. (2014). Eruption of South Sarigan Seamount in the Commonwealth of the Northern Mariana Islands: Insights into hazards from submarine volcanic eruptions. *Oceanography*, *27*(2), 24–31. https://doi.org/10.5670/oceanog.2014.37

Geller, R. J., & Mueller, C. S. (1980). Four similar earthquakes in central California. *Geophysical Research Letters*, *7*(10), 821–824. https://doi.org/10.1029/GL007i010p00821

Global Volcanism Program (1979). Report on Ahyi (United States). In D. Squires (Ed.), *Scientific Event Alert Network Bulletin*, *Smithsonian Institution*, (Vol. 4(11)). https://doi.org/10.5479/si.GVP.SEAN197911-284141

Global Volcanism Program (2001). Report on Ahyi (United States). In R. Wunderman (Ed.), *Bulletin of the Global Volcanism Network*, *Smithsonian Institution*, (Vol. 26(5)). https://doi.org/10.5479/si.GVP.BGVN200105-284141

Global Volcanism Program (2014). Report on Ahyi (United States). In R. Wunderman (Ed.), *Bulletin of the Global Volcanism Network*, *Smithsonian Institution*, (Vol. 39:2). https://doi.org/10.5479/si.GVP.BGVN201402-284141

Godin, O. A. (2007). Transmission of low-frequency sound through the water-to-air interface. *Acoustical Physics*, *53*(3), 305–312. https://doi.org/10.1134/S1063771007030074

Green, D. N., Evers, L. G., Fee, D., Matoza, R. S., Snellen, M., Smets, P., & Simons, D. (2013). Hydroacoustic, infrasonic and seismic monitoring of the submarine eruptive activity and sub-aerial plume generation at South Sarigan, May 2010. *Journal of Volcanology and Geothermal Research*, *257*, 31–43. https://doi.org/10.1016/j.jvolgeores.2013.03.006

Haney, M. M., Hotovec-Ellis, A. J., Bennington, N. L., de Angelis, S., & Thurber, C. (2014). Tracking changes in volcanic systems with seismic interferometry. In M. Beer, I. A. Kougioumtzoglou, E. Patelli, S.-K. Au (Eds.), *Encyclopedia of Earthquake Engineering* (pp. 3767–3786). Berlin, Heidelberg: Springer. https://doi.org/10.1007/978-3-642-36197-5_50-1

Haney, M. M., Van Eaton, A. R., Lyons, J. J., Kramer, R. L., Fee, D., & Iezzi, A. M. (2018). Volcanic thunder from explosive eruptions at Bogoslof volcano, Alaska. *Geophysical Research Letters*, *45*, 3429–3435. https://doi.org/10.1002/2017GL076911

Hanson, J., Le Bras, R., Dysart, P., Brumbaugh, D., Gault, A., & Guern, J. (2001). Operational processing of hydroacoustics at the Provisional International Data Center. *Pure and Applied Geophysics*, *158*(3), 425–456. https://doi.org/10.1007/PL00001190

Kokelaar, P. (1986). Magma-water interactions in subaqueous and emergent basaltic. *Bulletin of Volcanology*, *48*(5), 275–289. https://doi.org/10.1007/BF01081756

Lyons, J. J., Haney, M. M., Fee, D., & Paskievitch, J. F. (2014). Distinguishing high surf from volcanic long-period earthquakes. *Geophysical Research Letters*, *41*, 1171–1178. https://doi.org/10.1002/2013GL058954

Lyons, J. J., Haney, M. M., Werner, C., Kelly, P., Patrick, M., Kern, C., & Trusdell, F. (2016). Long period seismicity and very long period infrasound driven by shallow magmatic degassing at Mount Pagan, Mariana Islands. *Journal of Geophysical Research: Solid Earth*, *121*, 188–209. https://doi.org/10.1002/2015JB012490

McCreery, C., Oliveria, F., Walker, D., Hamada, N., & Talandier, J. (1989). Submarine volcano. *Eos Transactions American Geophysical Union*, *70*(45), 1466–1466. https://doi.org/10.1029/89EO00349

Metz, D., & Grevemeyer, I. (2018). Hydroacoustic measurements of the 2014 eruption at Ahyi volcano, 20.4°N Mariana Arc. *Geophysical Research Letters*, *45*, 11,050–11,058. https://doi.org/10.1029/2018GL079983

Metz, D., Watts, A. B., Grevemeyer, I., Rodgers, M., & Paulatto, M. (2016). Ultra-long-range hydroacoustic observations of submarine volcanic activity at Monowai, Kermadec Arc. *Geophysical Research Letters*, *43*, 1529–1536. https://doi.org/10.1002/2015GL067259

Moyer, C., and W. W. Chadwick Jr. (2017), Processed Acoustic Backscatter and Swath Bathymetry Data from the Izu-Bonin-Mariana Volcanic Arc acquired during R/V Roger Revelle expedition RR1413 (2014). Interdisciplinary Earth Data Alliance (IEDA). https://doi.org/10.1594/IEDA/324163

Norris, R. A., & Hart, D. N. (1970). Confirmation of Sofar-Hydrophone detection of submarine eruptions. *Journal of Geophysical Research*, *75*(11), 2144–2147. https://doi.org/10.1029/JB075i011p02144

Norris, R. A., & Johnson, R. H. (1969). Submarine volcanic eruptions recently located in the Pacific by SOFAR hydrophones. *Journal of Geophysical Research*, *74*(2), 650–664. https://doi.org/10.1029/JB074i002p00650

Okal, E. A. (2001). T-phase stations for the International Monitoring System of the Comprehensive Nuclear-Test Ban Treaty: A global perspective. *Seismological Research Letters*, *72*(2), 186–196. https://doi.org/10.1785/gssrl.72.2.186

Olson, J. V., & Szuberla, C. A. (2005). Distribution of wave packet sizes in microbarom wave trains observed in Alaska. *The Journal of the Acoustical Society of America*, *117*(3), 1032–1037. https://doi.org/10.1121/1.1854651

Resing, J. A., Baker, E. T., Lupton, J. E., Walker, S. L., Butterfield, D. A., Massoth, G. J., & Nakamura, K. (2009). Chemistry of hydrothermal plumes above submarine volcanoes of the Mariana Arc. *Geochemistry, Geophysics, Geosystems*, *10*, Q02009. https://doi.org/10.01029/02008GC002141

Resing, J. A., Rubin, K. H., Embley, R. W., Lupton, J. E., Baker, E. T., Dziak, R. P., et al. (2011). Active submarine eruption of boninite in the northeast Lau Basin. *Nature Geoscience*, *4*(11), 799–806. https://doi.org/10.1038/NGEO1275

Ryan, W. B. F., Carbotte, S. M., Coplan, J. O., O'Hara, S., Melkonian, A., Arko, R., et al. (2009). Global multi-resolution topography synthesis. *Geochemistry, Geophysics, Geosystems*, *10*, Q03014. https://doi.org/10.1029/2008GC002332

Schnur, S. R., Chadwick, W. W. Jr., Embley, R. W., Ferrini, V. L., de Ronde, C. E. J., Cashman, K. V., et al. (2017). A decade of volcanic construction and destruction at the summit of NW Rota-1 seamount: 2004–2014. *Journal of Geophysical Research: Solid Earth*, *122*, 1558–1584. https://doi.org/10.1002/2016JB013742

Searcy, C. (2013). Seismicity associated with the May 2010 eruption of South Sarigan Seamount, northern Mariana Islands. *Seismological Research Letters*, *84*(6), 1055–1061. https://doi.org/10.1785/0220120168

Stern, R. J. (2002). Subduction zones. *Reviews of Geophysics*, *40*(4), 1012. https://doi.org/10.1029/2001RG000108

Sugioka, H., Fukao, Y., & Hibiya, T. (2005). Submarine volcanic activity, ocean-acoustic waves and internal ocean tides. *Geophysical Research Letters*, *32*, L24616. https://doi.org/10.1029/2005GL024001

Talandier, J., & Okal, E. A. (1998). On the mechanism of conversion of seismic waves to and from T waves in the vicinity of island shores. *Bulletin of the Seismological Society of America*, *88*(2), 621–632.

Talandier, J., & Okal, E. A. (2016). A new source discriminant based on frequency dispersion for hydroacoustic phases recorded by T-phase stations. *Geophysical Journal International*, *206*(3), 1784–1794. https://doi.org/10.1093/gji/ggw249

Thompson, G., McNutt, S. R., & Tytgat, G. (2002). Three distinct regimes of volcanic tremor associated with the eruption of Shishaldin Volcano, Alaska 1999. *Bulletin of Volcanology*, *64*(8), 535–547. https://doi.org/10.1007/s00445-002-0228-z

Thompson, G., and C. Reyes (2018). GISMO—A seismic data analysis toolbox for MATLAB [software package], http://geoscience-community-codes.github.io/GISMO/, Accessed February 2018.

Watts, A. B., Peirce, C., Grevemeyer, I., Pauletto, M., Stratford, W. R., Bassett, D., et al. (2012). Rapid rates of growth and collapse of Monowai submarine volcano in the Kermadec Arc. *Nature Geoscience*, *5*(7), 510–515. https://doi.org/10.1038/ngeo1473

Waythomas, C. F., Haney, M. M., Fee, D., Schneider, D. J., & Wech, A. (2014). The 2013 eruption of Pavlof Volcano, Alaska: a spatter eruption at an ice-and snow-clad volcano. *Bulletin of Volcanology*, *76*(10), 862. https://doi.org/10.1007/s00445-014-0862-2

Wohletz, K. H. (1986). Explosive magma-water interactions: Thermodynamics, explosion mechanisms, and field studies. *Bulletin of Volcanology*, *48*(5), 245–264. https://doi.org/10.1007/BF01081754

Wright, I. C., Chadwick, W. W. Jr., de Ronde, C. E. J., Reymond, D., Hyvernaud, O., Gennerich, H.-H., et al. (2008). Collapse and reconstruction of Monowai submarine volcano, Kermadec arc, 1998-2004. *Journal of Geophysical Research*, *113*, B08S03. https://doi.org/10.1029/2007JB005138